Applied Surface Science 551 (2021) 149484

Contents lists available at ScienceDirect

Applied Surface Science

journal homepage: www.elsevier.com/locate/apsusc

Full Length Article

Enhanced hydrogen storage of a functional material: Hf_2CF_2 MXene with Li decoration

Aysenur Gencer [a], Sezgin Aydin [b], Ozge Surucu [c], Xiaotian Wang [d], Engin Deligoz [e], Gokhan Surucu [f,g,*]

[a] Karamanoglu Mehmetbey University, Department of Physics, Karaman 70100, Turkey
[b] Gazi University, Department of Physics, Ankara 06500, Turkey
[c] Atilim University, Department of Electrical and Electronics Engineering, Ankara 06836, Turkey
[d] Southwest University, School of Physical Science and Technology, Chongqing 400715, China
[e] Aksaray University, Department of Physics, Aksaray 68100, Turkey
[f] Middle East Technical University, Department of Physics, Ankara 06800, Turkey
[g] Ahi Evran University, Department of Electric and Energy, Kirsehir 40100, Turkey

ARTICLE INFO

Keywords:
Density functional theory
Hydrogen storage
Adsorption energy
Polarization mechanism
Charge transfer

ABSTRACT

In this paper, the hydrogen storage properties of the Li-decorated stable Hf_2CF_2 MXene layer, obtained by the exfoliation of Al from Hf_2AlC and F-termination, are considered by using first-principles calculations based on Density Functional Theory. First, the stability characteristics of the host structure (Hf_2CF_2 layer) are examined by investigating bulk Hf_2AlC. To enhance the adsorbed number of H_2 molecules, the well-defined initial H_2 coordinates are constructed by CLICH (Cap-Like Initial Conditions for Hydrogens) and Monte Carlo-based algorithms. After the geometry optimizations of the designed H_2 systems on the Li/Hf_2CF_2 layer, the adsorption energies of nH_2/Li/Hf_2CF_2 n = 1–10, 15, 20 and 25 systems are calculated, and the suitable values (0.2–0.6 eV/H_2) are obtained up to $15H_2$. For n = 20 and 25 systems, which have adsorption energies of 0.15 eV/H_2 and 0.16 eV/H_2, respectively. The structural properties and adsorption geometries of these molecules are analyzed. Additionally, the partial density of the states, electron density difference maps, and Mulliken atomic charges are presented to identify the actual binding mechanism of the systems. The results reveal that the Li-decorated Hf_2CF_2 MXene layer can be preferred for the hydrogen storage applications due to its stable nature and the convenient adsorption characteristics.

1. Introduction

Nowadays, energy consumption worldwide is steadily increasing owing to continuous industrial and technological developments. Such energy consumption calls for new resources; in this sense, fossil fuels still remain the most popular of all despite their limitations and drawbacks, namely the greenhouse effect and the global warming [1]. To tackle this problem, different alternatives, mostly renewable ones, are constantly sought after [2]. In this sense, the hydrogen-based energy has proved to be a promising source among the others because of its abundance, high density, environmentally friendliness, and other benefits [3]. However, one of the limitations of the hydrogen energy is storage of hydrogen since this gas has a very low density at ambient conditions. To solve this problem, several methods have been considered, namely gas storage, liquid storage and solid-state storage[4-8]. The gas hydrogen storage method requires high pressure tanks which necessitates advanced safety precautions [9]. As for the liquid hydrogen storage, extra energy is necessary to liquefy and keep the hydrogen at cryogenic temperature, after which stage another problem may arise known as boiling [9]. Besides these storage methods, hydrogen can also be stored physically or chemically in the solid-state method which is reversible and secure technique [10].

The physically solid-state hydrogen approach begins with hydrogen adsorption on the surface of a material; whereas, the chemical approach conducts hydrogen absorption in the material. Both of these methods should satisfy certain requirements such as high gravimetric storage capacity, reversible storage, hydrogen release at ambient conditions, etc. [11]. The US Department of Energy sets targets for these conditions.

* Corresponding author at: Middle East Technical University, Department of Physics, Ankara 06800, Turkey.
E-mail address: info@gokhansurucu.com (G. Surucu).

https://doi.org/10.1016/j.apsusc.2021.149484
Received 6 December 2020; Received in revised form 12 February 2021; Accepted 3 March 2021
Available online 7 March 2021
0169-4332/

Accordingly, the gravimetric storage capacity for light-duty vehicles is targeted as 5.5 wt% for 2025 [12]. Also, the average binding energy should be 0.2–0.6 eV/H_2 at room temperature for suitable adsorption and desorption processes [13]. In order to achieve these targets, several material groups have been investigated, such as magnesium based materials [14], complex hydrides [15], porous materials [16], nanotubes [17], graphene [18], two dimensional materials [19], and others. The chemically solid-state hydrogen storage method requires high temperature to release the stored hydrogen due to strong bonds between hydrogen and the material [20]. However, hydrogen release in the physically solid-state storage method occurs at low temperature due to the weak van der Waals force between the hydrogen atoms and the surface of the material.

The graphene [18], porous carbon material [16], and metal organic frameworks [21] groups have all been considered in the literature and meeting the high surface area requirement to store hydrogen while demanding low temperature due to the weak binding energy between the hydrogen and the surface of the material for practical applications [22]. In order to tackle this problem, metal decorations have been employed to increase the binding force and eliminate the low temperature requirement [23–25]; however, these decorations are prone to clustering [26]. Li and Na decorated graphdiyne was investigated and the binding energies of Li and Na atoms show that these atoms are dispersed on the graphydine and these systems are promising candidates for hydrogen storage applications [27]. In addition, the Li decorated Boron Hydride (BH) system was studied using DFT and it was found that Li decorated BH system has high storage capacity and reversible storage at ambient conditions [28]. Khosossi et al. studied the Li and Na doped boron phosphide and they found that Li binds strongly on the boron phosphide than Na with higher storage capacity [29]. As a result, the search for an efficient material for physically solid-state hydrogen storage continuous. In this vein, MAX phases having both metallic and ceramic properties are popular materials with high electrical and thermal conductivity, excellent damage tolerance, high oxidation resistance [30-32]; moreover, they could be exfoliated to 2-D materials as a new family called MXenes [33] which have unique properties such as a large surface area, high electronic conductivity, to mention a few [34-37]. As an example study from the literature, the Cr_2C MXene was investigated for hydrogen storage using Density Functional Theory [36] and the hydrogen atoms adsorbed various sites on the Cr_2C layer with suitable adsorption energies and high hydrogen storage capacities. Recently, Ti_2CT_x MXene [38] has been synthesized with different terminations as —F, —O and —OH and the hydrogen storage of this MXene has been analyzed and it shows the potential of this material for hydrogen storage applications due to high hydrogen storage capacity ~ 8 wt% under ~ 50–60 bar pressure. Generally, MXenes are obtained by the exfoliation of the A elements from the MAX phases [39]. Experimental studies reveal that this process results in surface terminations such as O, -F or —OH [33].

The motivation of the present study comes from the Hf_2C MXenes which, according to the literature, have the potential for obtaining surface terminations as O, -F or —OH with formation energies as −2.307 eV [40], −2.260 eV [41] and −1.439 eV [42] respectively. Because more negative values of formation energy imply more material stability, the O and F terminations can be considered when studying Hf_2C for their close formation energies. In the light above-mentioned background, the Li-decorated Hf_2C in the present work is considered for improved hydrogen storage capacity, and the surface termination is chosen as F due to the more stable bond between the F termination and Li decoration. In this sense, this work does not consider O termination due the strong bond between O and H preventing the latter's release. The results of the hydrogen adsorption on Hf_2CF_2 with Li decoration 2-D material are presented using geometric algorithms for hydrogen adsorption sides.

2. Calculation details

The density functional first-principles calculations were performed using the Vienna Ab-initio Simulation Package (VASP) [43,44] and the Cambridge Serial Total Energy Package (CASTEP) package [45]. The stability considerations and the band structure calculations of the bulk and layered systems were performed using VASP, and the hydrogen adsorption studies were executed using CASTEP and the Adsorption Locator module which supply effective tools and graphical interface. In addition, van der Waals correction was included in this study. For VASP calculations, the electron–electron interactions were considered using Perdew-Burke-Ernzerhof functional [46] within the Generalized Gradient Approximation (GGA) and the electron–ion interactions were considered using the Projector Augmented Wave (PAW) method [47,48]. Also, the energy cut-off was set to 600 eV, and k-point sampling was done with an 18 × 18 × 1 gamma-centered grid [49] for the unit cells. The energy and force convergences were performed up to 10^{-6} eV per unit cell and 10^{-5} eV/Å, respectively. In addition, the phonon dispersion curves were determined using Phonopy package [50] using the linear response method. For the CASTEP package calculations including the hydrogen adsorption processes, the Local Density Approximation (LDA) [51] functional is applied, since the van der Waals contributions and Coulombic interactions for metal-graphene systems can be modeled more efficiently using LDA [52-56]. The calculations were performed with 500 eV cut-off energy and 4 × 4 × 1 k-points for the 3 × 3 × 1 supercell including 45 atoms. Also, the ultrasoft pseudopotentials were used to describe the ion–electron interactions. The c axis was taken as 40 Å in all calculations to prevent any interactions between the layers. The initial H_2 positions were determined using the CLICH (Cap-Like Initial Conditions for Hydrogens) algorithm [57], by which the H_2 bond length is taken as 0.74 Å as the experimental value [58], θ is taken as 45° and z_{max} is taken as 3 Å. Also, r_{up} is set to 1 Å for the n = 1–6 systems to trigger interactions between the hydrogen molecules and Li. For the $n \geq 7$ systems, the radial distance between the H_2 molecules is fixed to h = 1.3 Å, instead of the fixed radius (r_{up}).

3. Results and discussions

3.1. Construction of Hf_2CF_2 layer

As shown in Fig. 1, Hf_2C could be obtained with the exfoliation of the Al element from Hf_2AlC (space group-P6_3/mmc, no:194). In this study, Hf_2C is considered with F termination due to the stability of Hf_2CF_2 (164 space group – P-3 m1). Table 1 lists the results of optimization for Hf_2AlC, all of which are consistent with the literature. After optimizing Hf_2AlC, Al is removed from the structure and F termination is added, resulting in crystal Hf_2CF_2. Hf_2CF_2 is optimized, the determined lattice parameters and formation energies appear in Table 1 as well. In the literature, Momeni Feili et al. [59] obtained the lattice parameter (a) and internal parameters for Hf and F. As can be seen from Table 1, the calculated parameters are consistent with Momeni Feili et al. [59].

Formation enthalpy is crucial in determining the thermodynamic stability and the synthesizability of a compound. For this purpose, Equation (1) is used for Hf_2CF_2 where $E_{Tot}^{Hf_2CF_2}$ is the total energy for Hf_2CF_2, and E_{Bulk}^{X} is the ground state energy for X element. According to Table 1, the negative formation energies of Hf_2AlC and Hf_2CF_2 compounds indicate thermodynamic stability and experimental synthesizability. It is also evident that the formation enthalpy of Hf_2CF_2 is more negative than that of Hf_2AlC, implying that Hf_2CF_2 is thermodynamically more stable than the latter.

$$\Delta E_f = E_{Tot}^{Hf_2CF_2} - \left(2 \times E_{Bulk}^{Hf} + E_{Bulk}^{C} + 2 \times E_{Bulk}^{F}\right) \quad (1)$$

The dynamical stability factor is crucial for hydrogen storage materials as well as their thermodynamic stability. In order to decide the dynamic stability of the material, the phonon dispersion calculations

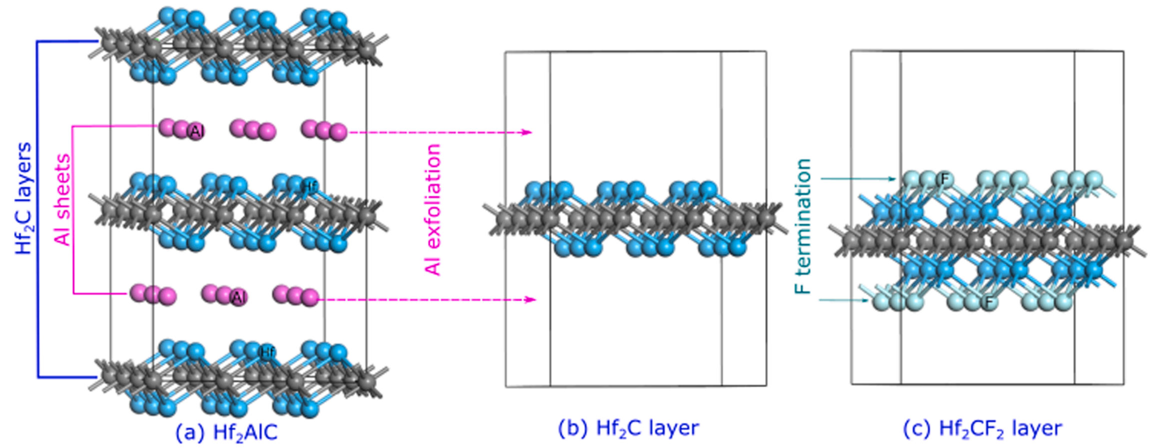

Fig. 1. Schematic representation of (a) 3x3x1 Hf_2AlC supercell (b) exfoliation to Hf_2C, and (c) Hf_2CF_2 layer obtained by F termination. Blue, gray, pink, and light green spheres stand for Hf, C, Al, and F atoms, respectively.

Table 1
Lattice parameters (*a* and *c*), formation energies (ΔE_f) and internal parameters (z) of the 3-D bulk Hf_2AlC and 2-D Hf_2CF_2.

Compound	a(Å)	c(Å)	ΔE_f(eV/atom)	z
Hf_2AlC	3.273	14.416	−0.756	0.086
	3.312 [60]	14.363 [60]		0.089 [60]
	3.212 [61]	14.383 [61]		0.086 [61]
Hf_2CF_2	3.268	20.094	−2.463	0.440 (Hf) 0.626 (F)
	3.203 [59]			0.0303 (Hf) [59]0.564 (F) [59]

must be performed. Fig. 2 shows the phonon dispersion curves and phonon density of states (PDOS) along the high symmetry points in the first Brillouin zone obtained by using the 2 × 2 × 1 and 3 × 3 × 1 supercells for Hf_2AlC and Hf_2CF_2, respectively. As can be seen from the figure, there are no negative frequencies, namely soft modes; in this way, both compounds are dynamically stable. In addition, there are more phonon branches for Hf_2CF_2 due to the higher number of atoms in its structure. Moreover carbon, as the lightest element in the structure, contributes to more to the higher frequencies of both compounds.

MAX-phases are metallic compounds, and MXenes as their 2-D derivatives also have metallic properties [62]. Fig. 3 shows the band structure and partial density of states (DOS) for Hf_2AlC and Hf_2CF_2. Accordingly, some bands are seen to cross the Fermi level thus indicating the metallic character of the compounds.

3.2. *Hydrogen adsorption properties of Li-Decorated Hf_2CF_2*

Because alkali decoration [23,63-66] enhances H_2 adsorption, the Hf_2CF_2 layer was decorated with a Li atom, and the 3 × 3 × 1 supercell of the Hf_2CF_2 layer including 18 Hf atoms, 9C atoms and 18F atoms was used to supply enough surface area for the adsorption processes. The Li element was chosen for this purpose due to its light mass. Fig. 4(a) and (b) show the side and top views of Li-decorated Hf_2CF_2, referred to here as Li/Hf_2CF_2. The top of the F atom (F1 site) was chosen as the initial Li position due to the stable bond between the layer/surface and the Li atoms. For metal decoration, the binding energy (E_{bind})[67,68] is used to determine the stability of the metal atom on the surface, and it can be calculated by

$$E_{bind} = E_{Li/Hf_2CF_2} - (E_{Hf_2CF_2} + E_{Li})$$

where $E_{Hf_2CF_2}$ is the total energy of Hf_2CF_2, E_{Li} is the total energy of the isolated Li atom, and E_{Li/Hf_2CF_2} is the total energy of Li decorated Hf_2CF_2. The binding energy of Li to the Hf_2CF_2 surface is calculated as −1.498 eV. The negative binding value shows the energetic stability, indicating that the Li atom is stable on the F1 site. In addition, the bond length between the F atom, which is terminating the surface, and the Li atom is 1.637 Å.

After Li decoration, the hydrogen adsorption properties were studied. For computational purposes, the construction of the initial co-

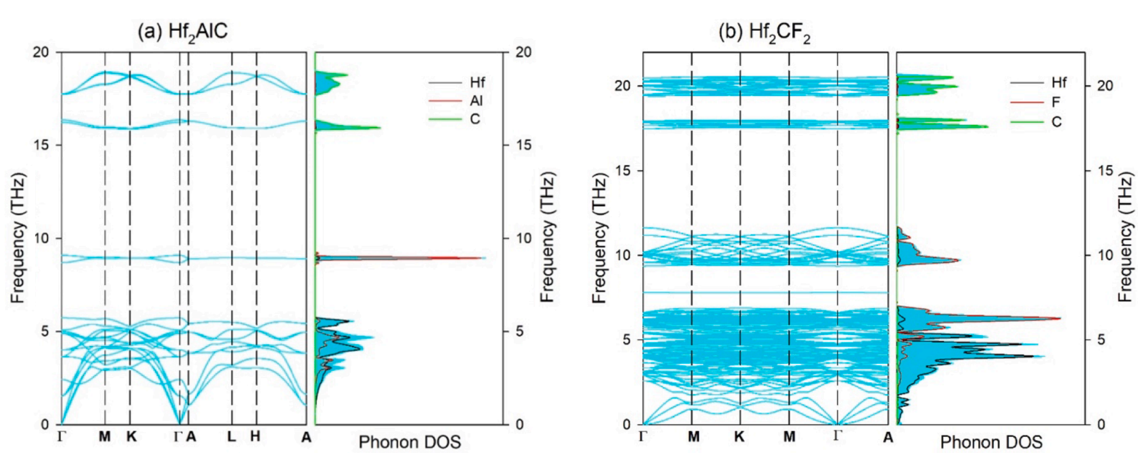

Fig. 2. Phonon dispersion curves and phonon density of states (PDOS) of Hf_2AlC (left) and Hf_2CF_2 (right).

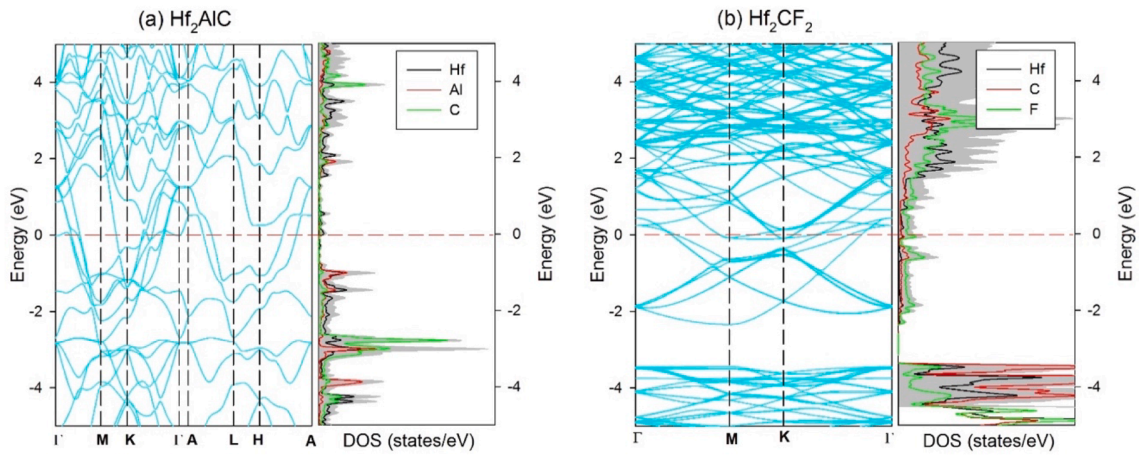

Fig. 3. Electronic band structures and density of states (a) Hf_2AlC and (b) Hf_2CF_2. The horizontal dashed red line represents the Fermi level set to 0 eV.

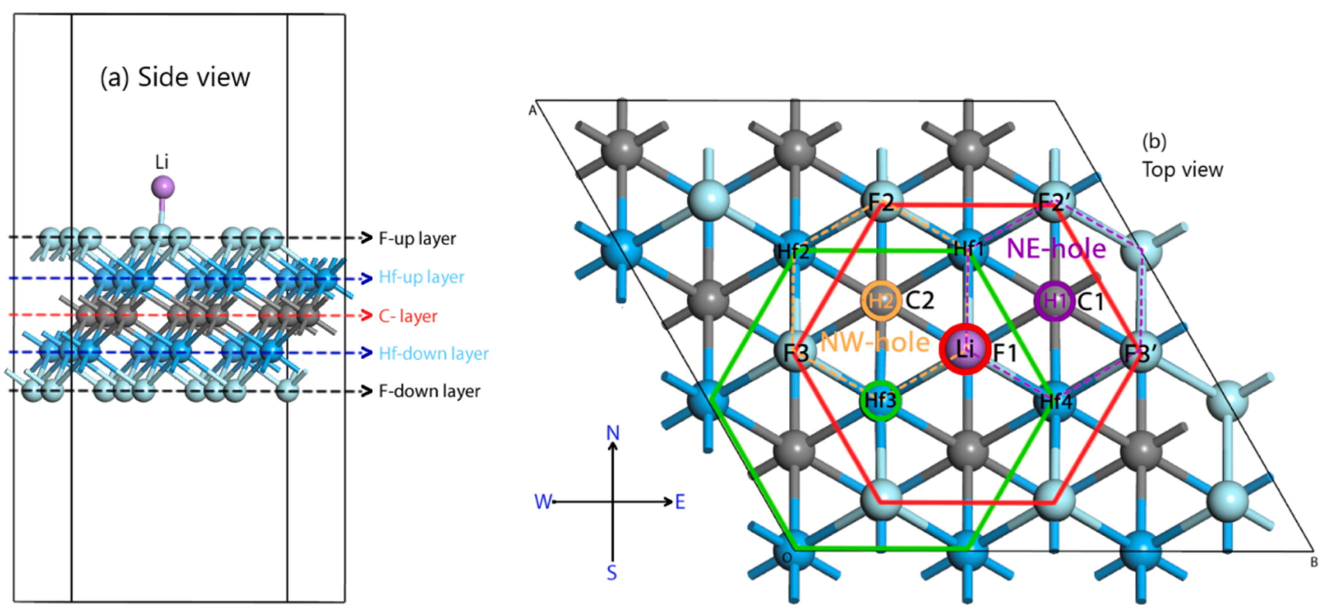

Fig. 4. Side view (a) and top view (b) of Li/Hf_2CF_2 with the site labels used in Mulliken charge analysis. The color representation for the atoms is the same as Fig. 1, and the purple sphere representing the Li atom. The F1 site is the bottom of the Li atom. The Hf, F and C atoms establish a filled hexagonal geometry in their own layers marked as solid green and red hexagons. The NW and NE holes are represented by dashed orange and purple hexagons.

ordinates of the system in point can be problematic, and poorly chosen coordinates can make the calculations and convergence difficult. Here, different solutions can be applied such as one-by-one addition, express calculations including different manual optimizations, and Monte-Carlo and adsorption locators [69-71]. A practical way to construct the initial coordinates of the H_2 molecules is to use the CLICH (Cap-Like Initial Conditions for Hydrogens) and RICH (Rotational Initial Conditions for Hydrogens) algorithms. See Aydin and Şimşek [57] for the details and advantages of these two algorithms. Using CLICH, the $nH_2/Li/Hf_2CF_2$ (n = 1–10) systems were designed. Alternatively, some systems were designed manually: one H_2 molecule was added to the optimized nH_2-adsorbed system, and new (n + 1) H_2 systems were constructed for n = 3–6 because there are a large number of adsorption scenarios as a result of possible interactions between H_2 molecules and the surface. Furthermore, to construct higher H_2-systems for n = 15, 20, and 25, the Adsorption Locator module in Materials Studio 6.0 was used [71] successfully to different physical problems [72-74]. All the designed systems were optimized using CASTEP. The adsorption energy is crucial for the hydrogen storage applications, and it should be in the range of 0.2–0.6 eV/H_2 for the system to be rendered acceptable [13,75,76]. For the optimized nH_2/Li/ Hf_2CF_2 (n = 1–10, 15, 20, and 25) systems, the adsorption energy (E_{ads}) [67,68] was calculated by

$$E_{ads} = -[E(nH_2/Li/Hf_2CF_2) - E(Li/Hf_2CF_2) - n \times E(H_2)]/n$$

where $E(nH_2/Li/Hf_2CF_2)$ is the total energy of the H_2-adsorbed system, $E(Li/Hf_2CF_2)$ is the total energy of the Li-decorated Hf_2CF_2 layer, $E(H_2)$ is the total energy of the H_2 molecule, and n is the number of H_2 molecules in the system. The calculated adsorption energies (E_{ads}, eV/H_2), and the structural properties including the distances between Li and Hf_2CF_2 [d(Li)], between H_2 and Li [d(Li-H_2)] in Å of the $nH_2/Li/Hf_2CF_2$ systems were listed in Table 2. Also, the distances between H_2 and Hf_2CF_2 [d(Hf_2CF_2-H_2)] and d(H_2) bond length in Å of the $nH_2/Li/Hf_2CF_2$ systems were listed in Supplementary Material Table S1. There, the Li/ Hf_2CF_2 systems can be seen to adsorb almost up to 15H_2 owing to the adsorption energies in the required range of 0.2–0.6 eV/H_2. In the literature, Li and Na decorated graphydine could adsorb up to 5H_2 molecule [27], Li decorated boron hydride could adsorb up to 4H_2 molecule [28] and one sided Li and Na decorated boron phosphide could adsorb up to 4H_2 molecule while double sided decorated boron

Table 2
The adsorption energies (E_{ads}, eV/H_2), the location of Li atom, and the distances d(Li) between Li and Hf_2CF_2, d(Li-H_2) between H_2 and Li (in Å) of nH_2/Li/Hf_2CF_2 systems. The n + 1 (n = 3, 4, 5, 6) systems are constructed manually with the adsorption of $1H_2$ to nH_2 system.

nH_2	d(Li)	d(Li-H_2) Min	d(Li-H_2) Max	E_{Ads}	Li location
1	0.904	2.020	2.119	1.06	NW-hole
2	0.929	2.052	3.109	0.59	NW-hole
3	0.938	2.055	3.736	0.46	NW-hole
3 + 1	0.968	2.100	3.817	0.39	NW-hole
4	0.943	2.008	3.902	0.38	NW-hole
4 + 1	0.964	2.037	4.030	0.34	NW-hole
5	0.956	2.079	4.139	0.34	NW-hole
5 + 1	0.966	2.074	4.230	0.30	NW-hole
6	0.980	2.006	4.516	0.27	NW-hole
6 + 1	0.982	1.985	4.486	0.25	NW-hole
7	1.647	4.313	4.422	0.04	F1 site
8	0.965	2.100	5.414	0.26	NW-hole
9	0.970	2.059	5.560	0.23	NW-hole
10	0.967	2.063	5.798	0.23	NW-hole
15	0.969	2.077	6.138	0.19	NE-hole
20	1.720	2.060	5.493	0.15	F1 site
25	1.705	2.031	6.049	0.16	F1 site

phosphide could adsorb up to $16H_2$ molecule [29]. Therefore, the adsorb $15H_2$ is a high hydrogen adsorption capacity in the Li/Hf_2CF_2 system. The adsorption energy decreases with the climbing number of H_2. Because the electrostatic interactions among the H_2 molecules due to increased H_2 concentration caused them to be dispersed over the layer, this distribution is supported by the increased d(Li-H_2) and d(Hf_2CF_2-H_2) with the increased number of H_2. Therefore, these H_2 molecules begin to interact with the open surface states, which are relatively weaker than the actual metal-H_2 bonds. However, $1H_2$/Li/Hf_2CF_2 has the highest adsorption energy, while nH_2/Li/Hf_2CF_2 (n = 20 and 25) systems have lower adsorption energies: thus, these do not satisfy the requirements. It was observed that the $7H_2$/Li/Hf_2CF_2 system designed by CLICH has a considerably low adsorption energy (0.04 eV/H_2), whereas the manually developed (6 + 1)H_2/Li/Hf_2CF_2 system is acceptable with 0.25 eV/H_2. Also, other manually constructed (n + 1) H_2/Li/Hf_2CF_2 systems have suitable adsorption energies. These lower adsorption energies obtained with CLICH could be explained with the interaction between the H_2 molecules that are repulsive electrostatic interactions and the H_2 molecules interaction with the decorated metal atom. These interactions are originated from the controlled initial co-ordinates and play a role in the adsorption process. However, in manually developed (n + 1)H_2/Li/Hf_2CF_2 systems, an additional H_2 molecule individually interacts with the metal atom after the nH_2 adsorption. Also, the repulsive interactions with the other H_2 molecules should not be as strong as in CLICH case. As a result, the latter can describe the alternative adsorption states. Furthermore, the d(Li) distance is 0.93–0.98 Å for the suitable systems. The lower distances (for the n = 1 system) correspond to the higher adsorption energy, while the higher ones (for the n = 7, 20 and 25 systems) correspond to the lower adsorption energy. The d(H_2) bond length is almost constant as 0.77 Å as can be seen from Table S1, indicating that the stretching of H-H bond due to the polarization is negligible, and the hydrogen atoms remain in the molecular state. Moreover, with the increased number of H_2 molecules, the Li atom moves to different locations on the layer due to the changing of the actual interactions and charge transfer. The Li atom located at the center of NW hole in nH_2/Li/Hf_2CF_2 [n = 1-(6 + 1), 8–10] systems, while it is located at the top of the F1 site for the n = 7, 20 and 25 systems. Finally, this atom remains only at the center of the NE hole for in the n = 15 system. Furthermore, Li atom energy profile for evenly spaced steps along the linear path from F1 to NW hole are shown in Fig. 5 to investigate Li atom migration on the layer in the presence of H_2 molecules. The NW hole is more stable than F1 site for Li atom as can be seen from Fig. 5. For the more detailed H_2 adsorption trends on the layer, and to examine not only metal interactions but also the effect of stable surface states such as NW hole on the H_2 adsorption process, Li atom was initially decorated to F1 site instead of the NW hole. Thus, in some cases, the H_2 molecules can interact with the empty NW hole. Also, the energy barrier of 5.0 meV between F1 and NW hole is very low. Thus, the Li atom can move from the initial F1 site to NW hole with H_2 adsorption.

To support the structural analysis presented above, the optimized geometries of the nH_2/Li/Hf_2CF_2 (n = 2–10, 15, 20, and 25) systems appear in Fig. 6. It is easily seen that some H_2 molecules accumulate around the metal atom, and interact with it. Some of them interact with the layer states as a result of increased repulsive interactions among the H_2 molecules, and prefer to diffuse over the surface. However, the d(Li-H_2) distance for the n = 1 system can be used as an adsorption criterion

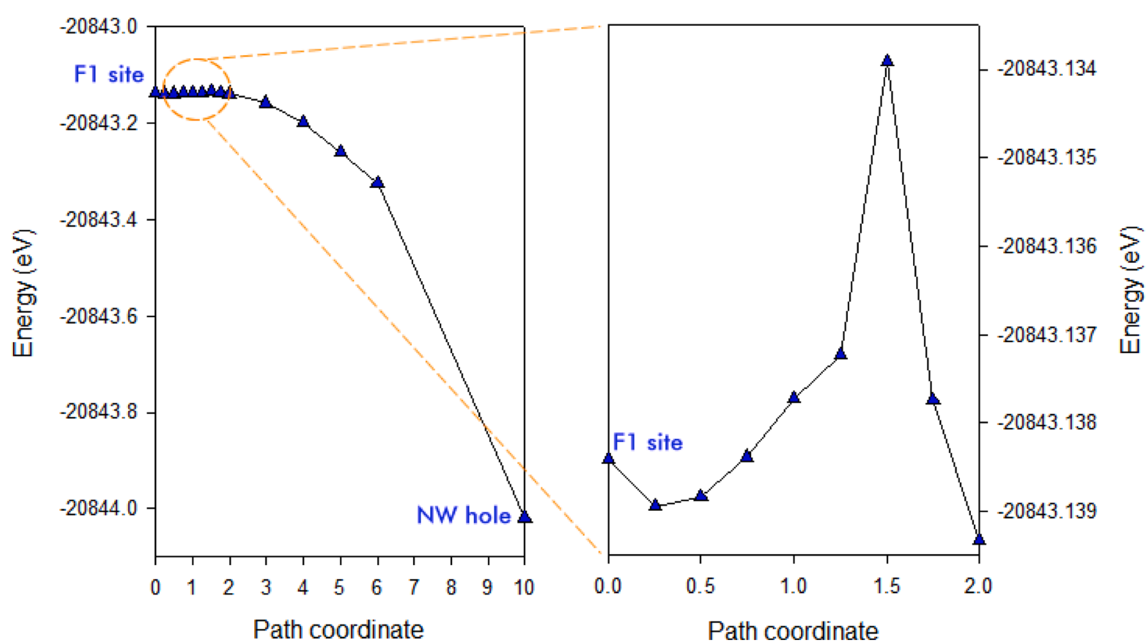

Fig. 5. Calculated Li atom energy profile along the linear path from F1 site to NW hole.

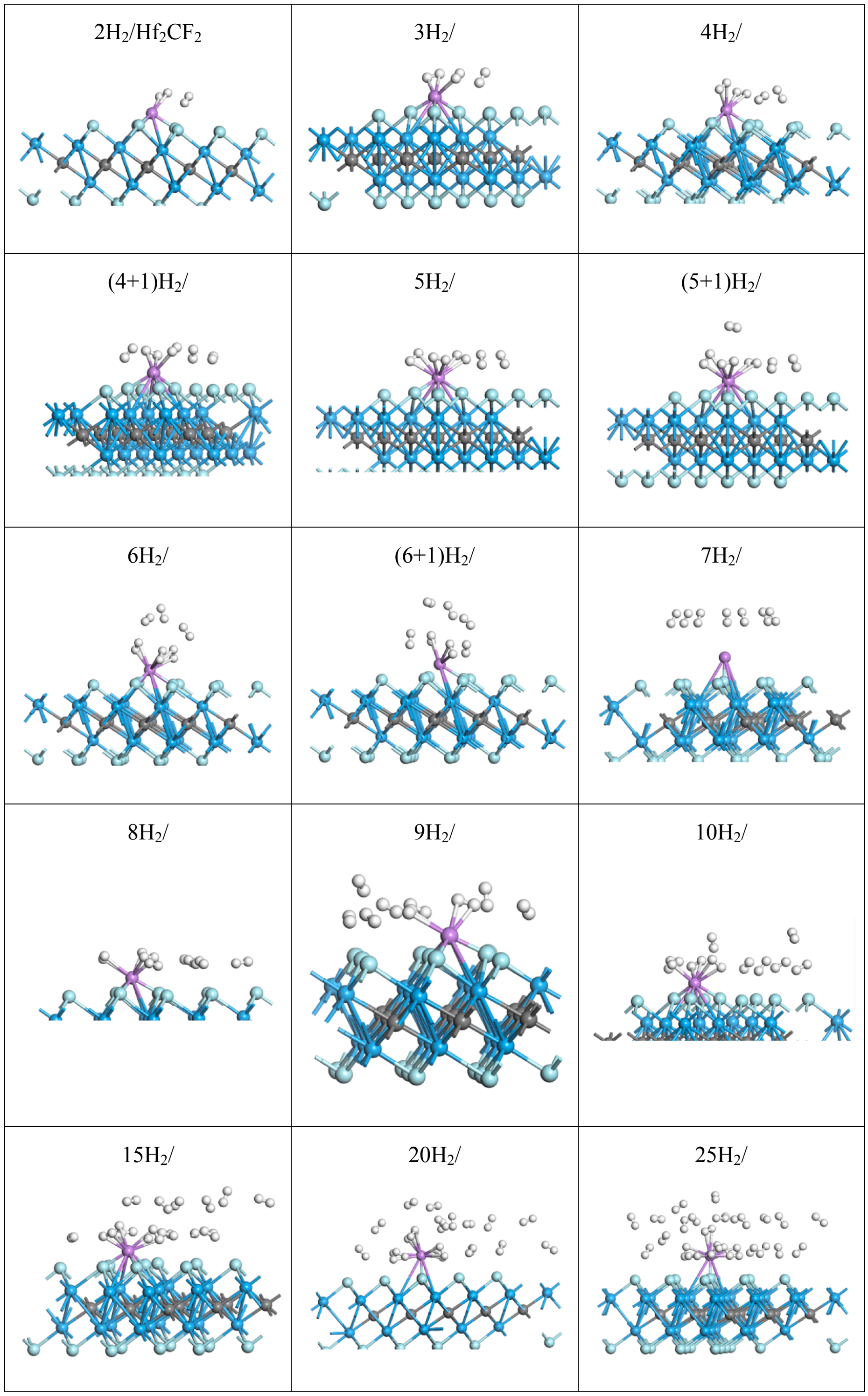

Fig. 6. Optimized geometries of the $nH_2/Li/Hf_2CF_2$ (n = 2–10, 15, 20, and 25) systems. The n + 1 (n = 3, 4, 5, 6) systems are constructed manually with the adsorption of $1H_2$ to nH_2 system.

for Li [77]. For example, the adsorbed maximum number of H_2 molecules per Li atom is 2 for n=(3, 4, and 9), 3 for n=(5, 8, and 10), and 5 for n=(20 and 25) systems.

Moreover, the partial density of states (PDOS) curves of Li/Hf_2CF_2 and the selected $nH_2/Li/Hf_2CF_2$ (n = 4, 6 and 8) systems are depicted in Fig. 7 to clarify and discuss the binding mechanism of H_2 on the Li-decorated Hf_2CF_2 layer. In addition, the adsorption processes are closely related to the possible charge transfers [55,63,78-80]. Therefore, the Mulliken atomic charges of the Li atom and H_2 molecules, as well as the transferred charge to the F-up and Hf-up layers in the $nH_2/Li/Hf_2CF_2$ systems were calculated, and the results were appeared in Table 3. From Fig. 7, the total PDOS of the down layers of the systems, named C+(F-down)+(Hf-down), almost remain unchanged with different numbers of H_2. This situation is supported by the Mulliken atomic charge analysis, and it is seen that the values of Q(F-up), Q(Hf-up), Q(F-down), Q(C) and Q(Hf-down) are −4.50*e*, 8.46*e*, −4.50*e*, −8.01*e*, and 8.46*e*, respectively.

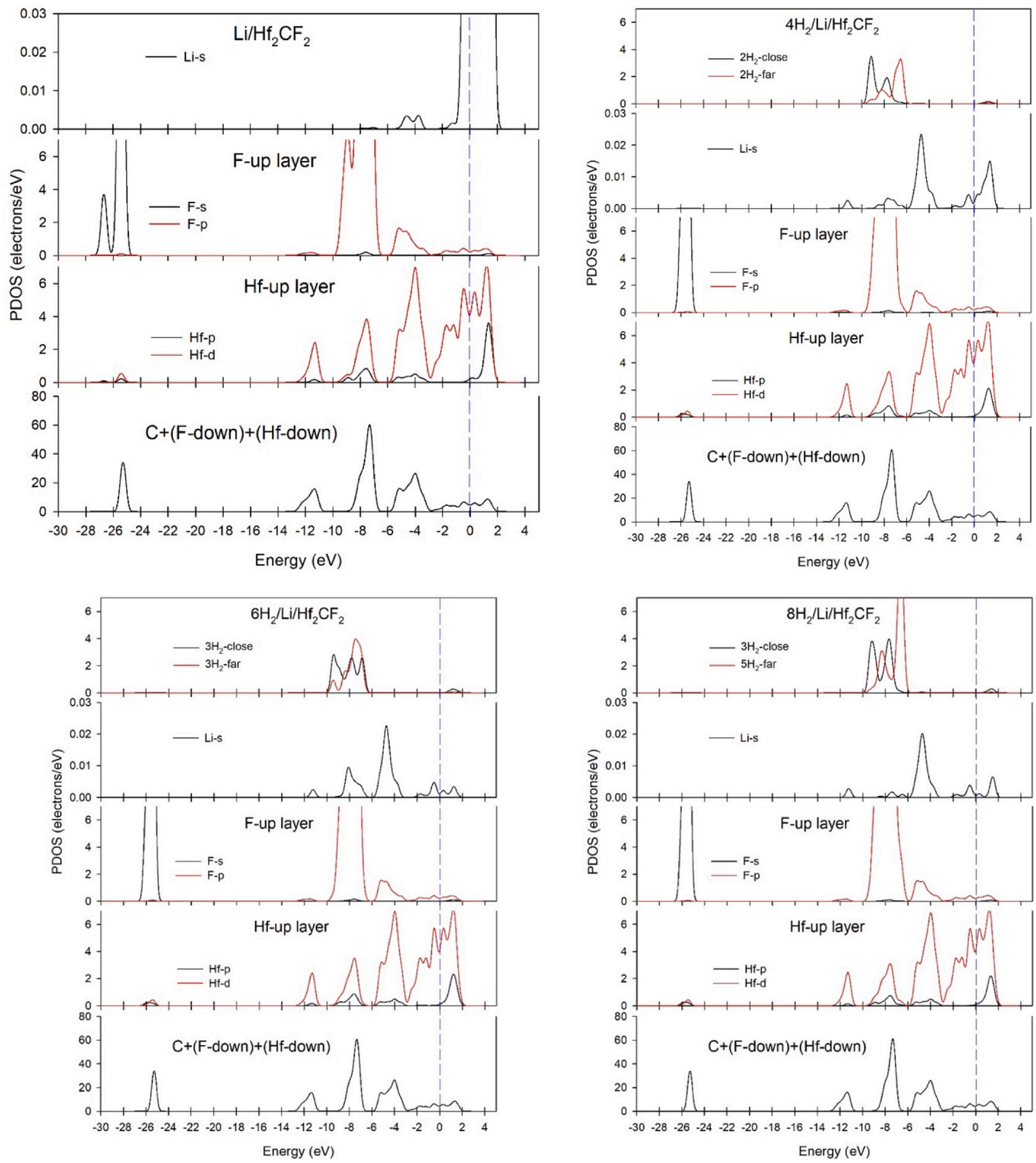

Fig. 7. The PDOS curves of Li/Hf_2CF_2 and the selected $nH_2/Li/Hf_2CF_2$ (n = 4, 6 and 8) systems.

Table 3
The hydrogen desorption temperatures (T_D in K) for $nH_2/Li/Hf_2CF_2$ systems that have required absorption energy between 0.2 and 0.6 eV/H_2.

nH_2	2	3	4	5	6	8	9	10	15
T_D	762	591	485	435	351	338	300	289	243

These values remain almost constant in all systems, implying that the down layers of Hf_2CF_2 system have no mature contributions to the surface interactions and H_2 adsorption processes. Additionally, from the computational perspective, these layers can be fixed for easier and faster convergence. However, the F-up and Hf-up layers are responsible for the actual interactions with the metal and H_2 molecules. From the PDOS of the Li/Hf_2CF_2 system, some resonant peaks for the Li and F-up layer are observed between −4 eV and the Fermi level, revealing possible hybridization between the Li and Hf_2CF_2 layer. There are also some resonant peaks of PDOS for the Hf-up-d states and F-up-p states between −8 eV and −6 eV with small contributions from the F-up-s and Hf-up-p states, indicating binding between the Hf-up and F-up layers. With hydrogen adsorption, the PDOS curves for Li and F-up changes due to the charge transfers. There are some small amplitude resonant peaks for the Li-s and s-states of the close H_2 molecules around −8 eV. These peaks indicate a weak hybridization between H_2 and Li. At the same time, the F-up-p states contribute to this hybridization with higher amplitude, thus concluding that the Li atom plays a bridging role between the Hf_2CF_2 layer and H_2 molecules. Also, there are some resonant peaks for the F-up-p and s-states of the H_2 molecules between −6 eV and −10 eV. These peaks indicate possible hybridization and strong binding between the H_2 and F-up layers, defining the binding of H_2 molecules that are not attached to metal and spread on the layer.

To present a detailed binding and charge transfer analysis from the Mulliken atomic charges listed in Supplementary Material Table S2, the Li atom transfers the charge and becomes a cation. The F layers are negatively charged, while the Hf layers are positively charged. Considering the charge deviations of the Li atom, F-up and Hf-up layers, T(F-up) and T(Hf-up), when the Li atom is attached to the layer, it gains + 0.76*e*, F-up layer gains −0.21*e* and Hf-up layer gains −0.54*e* charge. There is also a charge flow from Li to the F-up and Hf-up layers. A careful analysis of Table S2 reveals that the highest charge transfer to the F-up and Hf-up layers occurs in the $1H_2$-adsorbed system, resulting in the highest adsorption energy value. With the increased number of H_2 molecules, the transferred charge to the H_2 molecules increases, and the charge flow to the layers drops. This trend continuous up to the $(6H_2 + 1)$ system, after which, the induced electric field between the layers and the Li atom drops again; thus, the adsorption energy declines, i. e. the polarization mechanism of the H_2 molecules worsens. Furthermore, it is remarkable for the $n \leq (6H_2 + 1)$ systems that the transferred charge to the Hf-up layer, although it is geometrically farther away, is higher than the transferred charge to the F-up layer. This situation can be explained by the higher electron affinity of the Hf atoms and the lower ionization potential of the F atoms. For the $7H_2$ system, the transferred charge to the H_2 molecules is very low, therefore the adsorption energy is the lowest. With the $8H_2$ system, the transferred charge to the layers declines, and the transferred one to the H_2 molecules improves. This means the adsorption energy increases, thus satisfying the requirements. For the n = 15, 20 and 25 systems, the charge trend is a little different because the Hf up layer is more positive and the direction of the charge flow changes. This layer begins to transfer the charge to the upper side of the system. In this case, the total charge of the H_2 molecules becomes to increase, but the adsorption energy declines due to the reduced electric field.

Moreover, the given charge transfer mechanism between the layers can be expanded by the individual Mulliken atomic charges of the labeled sites, as defining in Fig. 4. It is noted here that the F1, F2, and F3, Hf1, Hf2 and Hf3 sites define the NW hole; while F1, F2′, and F3′, Hf1 and Hf4 define the NE hole. When all the individual atomic charges are considered, it is observed that Q(F2) and Q(F3), Q(F2′) and Q(F3′) are the same. Q(C1) and Q(C2) are the same as −089*e* in all systems. Only the different charges are listed in Table S2, where Q(F2′) is the same in terms of charge with the host structure, only changing in the $15H_2$ adsorbed system. This is because the Li atom prefers to move to the NE hole. Q(F1) is higher than the other F sites in the Li/Hf_2CF_2 and n = 7, 20, and 25 systems because the Li atom is located at the F1 site, and also the actual interactions between the Li and F1 atom are stronger than the other interactions. Furthermore, the charges of all Hf atoms shift with Li decoration and H_2 adsorption, exhibiting various trends due to the different binding mechanisms. Finally, it is concluded from the PDOS and Mulliken analysis mentioned earlier that there are two possible adsorption mechanisms for the H_2 on the Li/Hf_2CF_2 system: (i) hybridizations between the Li and H_2 molecules, and those between the F-up layer and H_2 molecules, (ii) polarization mechanism caused by the charge transfer between the Li and the Hf_2CF_2 layer, namely the induced electric field, which is one of the main interactions in this type of systems [53,63,78,79,81,82].

On the other hand, the discussed charge transfers can be easily supported by electron density difference (EDF, ρ_{diff}). The EDFs of the Li/Hf_2CF_2 and $nH_2/Li/Hf_2CF_2$ (n = 4, 6, and 8) systems were calculated by

$$\rho_{diff} = \rho_{nH_2/Li/Hf_2CF_2} - \rho_{Li/Hf_2CF_2} - \rho_{Li} - \rho_{nH_2}$$

where $\rho_{nH_2/Li/Hf_2CF_2}$ and ρ_{Li/Hf_2CF_2} are the charge density of the nH_2-adsorbed system and the metal-decorated system, respectively. ρ_{Li} and ρ_{nH_2} are the charge density of the metal atom and the adsorbed nH_2 molecules, respectively. The calculated 3D EDFs were depicted in Fig. 8 where the blue-colored regions represent electron accumulation (- regions) while the yellow-colored regions represent electron depletion (+regions). The metal Li creates a spherical positive charge distribution (the yellow region in Fig. 8(a)), and there is a charge transfer between the Li and F-up and Hf-up layers (the blue colored regions). With the H_2 adsorption, one side of the H_2 molecules is blue colored, and the other side is yellow colored, see Fig. 8(b)-(d). This indicates the polarization of the H_2 molecules. The F-up layer is negatively charged, and it can be interacted with the polarized H_2 molecules.

3.3. Hydrogen storage characteristics of Li-Decorated Hf_2CF_2

The previous sections present the hydrogen adsorption on Li decorated Hf_2CF_2 MXene and the hydrogen storage characteristics are crucial consideration for the practical applications. For the hydrogen adsorb systems, the desorption temperature being one of the characteristics could be estimated using van't Hoff equation [83,84] as

$$T_D = \frac{E_{Ads}}{k_B}\left(\frac{\Delta S}{R} - lnP\right)^{-1}$$

where T_D is the desorption temperature, E_{Ads} is the adsorption energy, k_B is the Boltzmann constant, R is the universal gas constant, P is equilibrium pressure taken as 1 atm and ΔS is the entropy change of hydrogen taken as 75.44 $Jmol^{-1}K^{-1}$ [84]. In order to have a desorption at ambient conditions, the adsorption energy is crucial. and should be in the range of 0.2–0.6 eV/H_2 for hydrogen storage systems. As listed in Table 2, all the $nH_2/Li/Hf_2CF_2$ systems do not have the adsorption energies in this required range, therefore the $nH_2/Li/Hf_2CF_2$ systems that have suitable adsorption energies are considered for the desorption temperature determination. Table 3 lists the estimated desorption temperatures for $nH_2/Li/Hf_2CF_2$ systems. As can be concluded from Table 3, the hydrogen release could occur at ambient conditions with the increasing number of H_2 molecules on the $nH_2/Li/Hf_2CF_2$ systems due to the lower adsorption energy for the H_2 molecules and the $9H_2$ system has a desorption temperature close to the room temperature.

The gravimetric storage capacity is another characteristic of the hydrogen adsorb systems related to the adsorption capacity and it is the amount of hydrogen storage per unit mass of the material. In order to have a high storage capacity, the number of adsorb H_2 should be high. For $nH_2/Li/Hf_2CF_2$ systems, the highest capacity is obtained for n = $15H_2$ system. But these two characteristics should be considered at the same time for practical applications. The n = $15H_2$ system has a low desorption temperature despite having high storage capacity and it is not a feasible system for real-life applications. The $9H_2$ system could be a potential candidate for real-life application with having suitable desorption temperature and a high storage capacity.

4. Conclusion

After the stability of the Hf_2CF_2 layer was checked by the calculated formation enthalpy and phonon dispersion curves, the nH_2 adsorption characteristics of the Li-decorated Hf_2CF_2 layer for n = 1–10, 15, 20 and 25 were investigated by first-principles density functional calculations. From the calculated adsorption energy values, it can be seen that the Li/Hf_2CF_2 systems can adsorb almost up to $15H_2$ with the acceptable

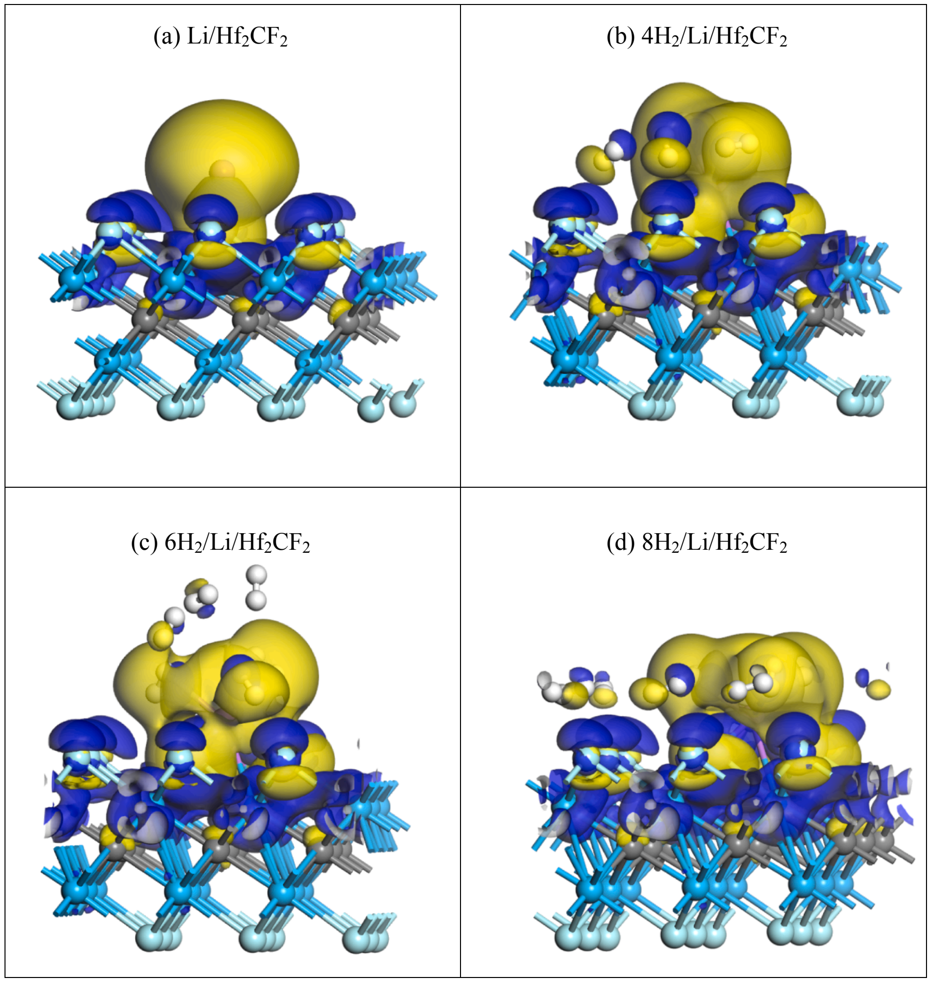

Fig. 8. Top view of the calculated electron density differences for the Li/Hf_2CF_2 and $nH_2/Li/Hf_2CF_2$ (n = 4, 6, and 8) systems. The isosurface value is 0.004 e/Å^3. The blue colored regions represent electron accumulation while the yellow-colored regions represent electron depletion.

adsorption energies (0.2–0.6 eV/H_2). With the increased number of H_2, the Li atom moves to different locations on the layer, and the adsorption energy decreases due to changes in the actual charge transfer mechanism and different H_2 interactions with the layer. Some H_2 molecules interact with the metal, while some of them spread over the surface and interact with the F layer. To reveal the key binding/adsorption mechanisms and to support them, partial density of states, Mulliken atomic charges and electron density differences were calculated. It is concluded that there are two possible mechanisms, calling one is the hybridizations between the Li and H_2 molecules, as well as between F-up layer and H_2 molecules; the other one is the well-known polarization mechanism caused by the charge transfer between the Li and the layer, namely the induced electric field. Finally, this type of MXenes exhibits high structural stability and effective ionic surface and charge transfer capability, thereby leading to enhanced H_2 adsorption qualities. Considering the popularity of the MXene systems recently, hydrogen storage can be a new research area for this family of materials.

CRediT authorship contribution statement

Aysenur Gencer: Writing - original draft, Data curation, Validation. **Sezgin Aydin:** Writing - original draft, Methodology, Data curation, Software. **Ozge Surucu:** Writing - review & editing, Investigation. **Xiaotian Wang:** Writing - review & editing. **Engin Deligoz:** Writing - review & editing, Formal analysis. **Gokhan Surucu:** Conceptualization, Methodology, Writing - review & editing, Software.

Declaration of Competing Interest

The authors declare that they have no known competing financial interests or personal relationships that could have appeared to influence the work reported in this paper.

Acknowledgment

The calculations were partially performed at TUBITAK ULAKBIM, High Performance and Grid Computing Center (TRUBA resources). Also, some parts of the calculations were performed at the high-performance computing center (HPCC) of Gazi University

Appendix A. Supplementary material

Supplementary data to this article can be found online at https://doi.org/10.1016/j.apsusc.2021.149484.

References

[1] F. Martins, C. Felgueiras, M. Smitkova, N. Caetano, Analysis of Fossil Fuel Energy Consumption and Environmental Impacts in European Countries, Energies. 12 (2019) 964, https://doi.org/10.3390/en12060964.
[2] S.R. Sinsel, R.L. Riemke, V.H. Hoffmann, Challenges and solution technologies for the integration of variable renewable energy sources—a review, Renew. Energy. 145 (2020) 2271–2285, https://doi.org/10.1016/j.renene.2019.06.147.
[3] J.O. Abe, A.P.I. Popoola, E. Ajenifuja, O.M. Popoola, Hydrogen energy, economy and storage: Review and recommendation, Int. J. Hydrogen Energy. 44 (2019) 15072–15086, https://doi.org/10.1016/j.ijhydene.2019.04.068.

[4] L. Ouyang, F. Liu, H. Wang, J. Liu, X.S. Yang, L. Sun, M. Zhu, Magnesium-based hydrogen storage compounds: A review, J. Alloys Compd. 832 (2020), 154865, https://doi.org/10.1016/j.jallcom.2020.154865.
[5] N.Z. Nurul, Z. Yaakob, K.L. Lim, S.N. Timmiati, The kinetics of lightweight solid-state hydrogen storage materials: A review, Int. J. Hydrogen Energy. 41 (2016) 13131–13151, https://doi.org/10.1016/j.ijhydene.2016.05.169.
[6] N.A.A. Rusman, M. Dahari, A review on the current progress of metal hydrides material for solid-state hydrogen storage applications, Int. J. Hydrogen Energy. 41 (2016) 12108–12126, https://doi.org/10.1016/j.ijhydene.2016.05.244.
[7] K.K. Gangu, S. Maddila, S.B. Mukkamala, S.B. Jonnalagadda, Characteristics of MOF, MWCNT and graphene containing materials for hydrogen storage: A review, J. Energy Chem. 30 (2019) 132–144, https://doi.org/10.1016/j.jechem.2018.04.012.
[8] R. Moradi, K.M. Groth, Hydrogen storage and delivery: Review of the state of the art technologies and risk and reliability analysis, Int. J. Hydrogen Energy 44 (2019) 12254–12269, https://doi.org/10.1016/j.ijhydene.2019.03.041.
[9] B. Sakintuna, F. Lamari-Darkrim, M. Hirscher, Metal hydride materials for solid hydrogen storage: A review, Int. J. Hydrogen Energy 32 (2007) 1121–1140, https://doi.org/10.1016/j.ijhydene.2006.11.022.
[10] G. Walker, Hydrogen storage technologies, in: Solid-State Hydrog. Storage Mater. Chem., Elsevier Inc., 2008: pp. 3–17. https://doi.org/10.1533/9781845694944.1.3.
[11] D.P. Broom, Hydrogen sorption properties of materials, Green Energy Technol. 27 (2011) 61–115, https://doi.org/10.1007/978-0-85729-221-6_3.
[12] DOE Technical Targets for Onboard Hydrogen Storage for Light-Duty Vehicles | Department of Energy, (n.d.). https://www.energy.gov/eere/fuelcells/doe-technical-targets-onboard-hydrogen-storage-light-duty-vehicles (accessed April 30, 2020).
[13] Y.H. Kim, Y. Zhao, A. Williamson, M.J. Heben, S.B. Zhang, Nondissociative adsorption of H2 molecules in light-element-doped fullerenes, Phys. Rev. Lett. 96 (2006), 016102, https://doi.org/10.1103/PhysRevLett.96.016102.
[14] Y. Sun, C. Shen, Q. Lai, W. Liu, D.W. Wang, K.F. Aguey-Zinsou, Tailoring magnesium based materials for hydrogen storage through synthesis: Current state of the art, Energy Storage Mater. 10 (2018) 168–198, https://doi.org/10.1016/j.ensm.2017.01.010.
[15] I.P. Jain, P. Jain, A. Jain, Novel hydrogen storage materials: A review of lightweight complex hydridespuye, J. Alloys Compd. 503 (2010) 303–339, https://doi.org/10.1016/j.jallcom.2010.04.250.
[16] Y. Xia, Z. Yang, Y. Zhu, Porous carbon-based materials for hydrogen storage: Advancement and challenges, J. Mater. Chem. A. 1 (2013) 9365–9381, https://doi.org/10.1039/c3ta10583k.
[17] A.C. Dillon, K.M. Jones, T.A. Bekkedahl, C.H. Kiang, D.S. Bethune, M.J. Heben, Storage of hydrogen in single-walled carbon nanotubes, Nature. 386 (1997) 377–379, https://doi.org/10.1038/386377a0.
[18] X. Wu, Y. Pei, X.C. Zeng, B_2C graphene, nanotubes, and nanoribbons, Nano Lett. 9 (2009) 1577–1582, https://doi.org/10.1021/nl803758s.
[19] A. Hashmi, M.U. Farooq, I. Khan, J. Son, J. Hong, Ultra-high capacity hydrogen storage in a Li decorated two-dimensional C_2N layer, J. Mater. Chem. A 5 (2017) 2821–2828, https://doi.org/10.1039/c6ta08924k.
[20] G. Walker, Solid-state hydrogen storage: Materials and chemistry, Elsevier Inc., 2008. https://doi.org/10.1533/9781845694944 .
[21] A. Ahmed, S. Seth, J. Purewal, A.G. Wong-Foy, M. Veenstra, A.J. Matzger, D. J. Siegel, Exceptional hydrogen storage achieved by screening nearly half a million metal-organic frameworks, Nat. Commun. 10 (2019) 1–9, https://doi.org/10.1038/s41467-019-09365-w.
[22] T.K.A. Hoang, D.M. Antonelli, Exploiting the Kubas Interaction in the Design of Hydrogen Storage Materials, Adv. Mater. 21 (2009) 1787–1800, https://doi.org/10.1002/adma.200802832.
[23] P. Panigrahi, A.K. Dhinakaran, S.R. Naqvi, S.R. Gollu, R. Ahuja, T. Hussain, Light metal decorated graphdiyne nanosheets for reversible hydrogen storage, Nanotechnology. 29 (2018), 355401, https://doi.org/10.1088/1361-6528/AAC84C.
[24] L. Wang, X. Chen, H. Du, Y. Yuan, H. Qu, M. Zou, First-principles investigation on hydrogen storage performance of Li, Na and K decorated borophene, Appl. Surf. Sci. 427 (2018) 1030–1037, https://doi.org/10.1016/j.apsusc.2017.08.126.
[25] S. Kumar, T.J. Dhilip Kumar, Electronic Structure Calculations of Hydrogen Storage in Lithium-Decorated Metal-Graphyne Framework, ACS Appl. Mater. Interf. 9 (2017) 28659–28666, https://doi.org/10.1021/acsami.7b09893.
[26] Q. Sun, Q. Wang, P. Jena, Y. Kawazoe, Clustering of Ti on a C60 surface and its effect on hydrogen storage, J. Am. Chem. Soc. 127 (2005) 14582–14583, https://doi.org/10.1021/ja0550125.
[27] Y. Wang, G. Xu, S. Deng, Q. Wu, Z. Meng, X. Huang, L. Bi, Z. Yang, R. Lu, Lithium and sodium decorated graphdiyne as a candidate for hydrogen storage: First-principles and grand canonical Monte Carlo study, Appl. Surf. Sci. 509 (2020), 144855, https://doi.org/10.1016/j.apsusc.2019.144855.
[28] L. Chen, X. Chen, C. Duan, Y. Huang, Q. Zhang, B. Xiao, Reversible hydrogen storage in pristine and Li decorated 2D boron hydride, Phys. Chem. Chem. Phys. 20 (2018) 30304–30311, https://doi.org/10.1039/c8cp05846f.
[29] N. Khossossi, Y. Benhouria, S.R. Naqvi, P.K. Panda, I. Essaoudi, A. Ainane, R. Ahuja, Hydrogen storage characteristics of Li and Na decorated 2D boron phosphide, Sustain. Energy Fuels. 4 (2020) 4538–4546, https://doi.org/10.1039/d0se00709a.
[30] J. Gonzalez-Julian, G. Mauer, D. Sebold, D.E. Mack, R. Vassen, Cr_2AlC MAX phase as bond coat for thermal barrier coatings: Processing, testing under thermal gradient loading, and future challenges, J. Am. Ceram. Soc. 103 (2020) 2362–2375, https://doi.org/10.1111/jace.16935.
[31] S. Jin, T. Su, Q. Hu, A. Zhou, Thermal conductivity and electrical transport properties of double-A-layer MAX phase Mo_2Ga_2C, Mater. Res. Lett. 8 (2020) 158–164, https://doi.org/10.1080/21663831.2020.1724204.
[32] D.W. Clark, S.J. Zinkle, M.K. Patel, C.M. Parish, High temperature ion irradiation effects in MAX phase ceramics, Acta Mater. 105 (2016) 130–146, https://doi.org/10.1016/j.actamat.2015.11.055.
[33] G.Y. Anasori Babak (Ed.), 2D Metal Carbides and Nitrides (MXenes), Springer International Publishing, 2019, https://doi.org/10.1007/978-3-030-19026-2.
[34] B.M. Jun, S. Kim, J. Heo, C.M. Park, N. Her, M. Jang, Y. Huang, J. Han, Y. Yoon, Review of MXenes as new nanomaterials for energy storage/delivery and selected environmental applications, Nano Res. 12 (2019) 471–487, https://doi.org/10.1007/s12274-018-2225-3.
[35] Q. Hu, H. Wang, Q. Wu, X. Ye, A. Zhou, D. Sun, L. Wang, B. Liu, J. He, Two-dimensional Sc_2C: A reversible and high-capacity hydrogen storage material predicted by first-principles calculations, Int. J. Hydrogen Energy. 39 (2014) 10606–10612, https://doi.org/10.1016/j.ijhydene.2014.05.037.
[36] A. Yadav, A. Dashora, N. Patel, A. Miotello, M. Press, D.C. Kothari, Study of 2D MXene Cr_2C material for hydrogen storage using density functional theory, Appl. Surf. Sci. 389 (2016) 88–95, https://doi.org/10.1016/j.apsusc.2016.07.083.
[37] Q. Hu, D. Sun, Q. Wu, H. Wang, L. Wang, B. Liu, A. Zhou, J. He, MXene: A new family of promising hydrogen storage medium, J. Phys. Chem. A. 117 (2013) 14253–14260, https://doi.org/10.1021/jp409585v.
[38] S. Liu, J. Liu, X. Liu, J. Shang, L. Xu, R. Yu, J. Shui, Hydrogen storage in incompletely etched multilayer Ti_2CTx at room temperature, Nat. Nanotechnol. (2021) 1–6, https://doi.org/10.1038/s41565-020-00818-8.
[39] K. Hantanasirisakul, Y. Gogotsi, Electronic and Optical Properties of 2D Transition Metal Carbides and Nitrides (MXenes), Adv. Mater. 30 (2018) 1804779, https://doi.org/10.1002/adma.201804779.
[40] CHf2O2 - Summary, (n.d.). https://cmrdb.fysik.dtu.dk/c2db/row/CHf2O2-27e68f9f2aef (accessed May 10, 2020).
[41] CF2Hf2 - Summary, (n.d.). https://cmrdb.fysik.dtu.dk/c2db/row/CF2Hf2-94a628f74b1f (accessed May 10, 2020).
[42] CH2Hf2O2 - Summary, (n.d.). https://cmrdb.fysik.dtu.dk/c2db/row/CH2Hf2O2-f4ccf972e8da (accessed May 10, 2020).
[43] G. Kresse, J. Furthmüller, Efficient iterative schemes for ab initio total-energy calculations using a plane-wave basis set, Phys. Rev. B - Condens. Matter Mater. Phys. 54 (1996) 11169–11186, https://doi.org/10.1103/PhysRevB.54.11169.
[44] G. Kresse, J. Furthmüller, Efficiency of ab-initio total energy calculations for metals and semiconductors using a plane-wave basis set, Comput. Mater. Sci. 6 (1996) 15–50, https://doi.org/10.1016/0927-0256(96)00008-0.
[45] S.J. Clark, M.D. Segall, C.J. Pickard, P.J. Hasnip, M.I.J. Probert, K. Refson, M. C. Payne, First principles methods using CASTEP, Zeitschrift Fur Krist. 220 (2005) 567–570, https://doi.org/10.1524/zkri.220.5.567.65075.
[46] J.P. Perdew, K. Burke, M. Ernzerhof, Generalized gradient approximation made simple, Phys. Rev. Lett. 77 (1996) 3865–3868, https://doi.org/10.1103/PhysRevLett.77.3865.
[47] G. and J.D. Kresse, From ultrasoft pseudopotentials to the projector augmented-wave method, Phys. Rev. B - Condens. Matter Mater. Phys. 59 (1999) 1758–1775. https://doi.org/10.1103/PhysRevB.59.1758 .
[48] P.E. Blöchl, Projector augmented-wave method, Phys. Rev. B. 50 (1994) 17953–17979, https://doi.org/10.1103/PhysRevB.50.17953.
[49] J.D. Pack, H.J. Monkhorst, "special points for Brillouin-zone integrations"-a reply, Phys. Rev. B. 16 (1977) 1748–1749, https://doi.org/10.1103/PhysRevB.16.1748.
[50] A. Togo, I. Tanaka, First principles phonon calculations in materials science, Scr. Mater. 108 (2015) 1–5, https://doi.org/10.1016/j.scriptamat.2015.07.021.
[51] J.P. Perdew, Y. Wang, Accurate and simple analytic representation of the electron-gas correlation energy, Phys. Rev. B. 45 (1992) 13244–13249, https://doi.org/10.1103/PhysRevB.45.13244.
[52] H. Zhang, M. Zhao, H. Bu, X. He, M. Zhang, L. Zhao, Y. Luo, Ultra-high hydrogen storage capacity of Li-decorated graphyne: A first-principles prediction, J. Appl. Phys. 112 (2012), 084305, https://doi.org/10.1063/1.4759235.
[53] Y. Guo, K. Jiang, B. Xu, Y. Xia, J. Yin, Z. Liu, Remarkable hydrogen storage capacity in Li-decorated graphyne: Theoretical predication, J. Phys. Chem. C. 116 (2012) 13837–13841, https://doi.org/10.1021/jp302062c.
[54] Y. Okamoto, Y. Miyamoto, Ab initio investigation of physisorption of molecular hydrogen on planar and curved graphenes, J. Phys. Chem. B. 105 (2001) 3470–3474, https://doi.org/10.1021/jp003435h.
[55] S. Seenithurai, R.K. Pandyan, S.V. Kumar, C. Saranya, M. Mahendran, Li-decorated double vacancy graphene for hydrogen storage application: A first principles study, Int. J. Hydrogen Energy. 39 (2014) 11016–11026, https://doi.org/10.1016/j.ijhydene.2014.05.068.
[56] M. Li, Y. Li, Z. Zhou, P. Shen, Z. Chen, Ca-Coated boron fullerenes and nanotubes as superior hydrogen storage materials, Nano Lett. 9 (2009) 1944–1948, https://doi.org/10.1021/nl900116q.
[57] S. Aydin, M. Şimşek, The enhancement of hydrogen storage capacity in Li, Na and Mg-decorated BC_3 graphene by CLICH and RICH algorithms, Int. J. Hydrogen Energy. 44 (2019) 7354–7370, https://doi.org/10.1016/j.ijhydene.2019.01.222.
[58] H.T. Chen, Y.M. Choi, M. Liu, M.C. Lin, A theoretical study of surface reduction mechanisms of CeO_2(111) and (110) by H_2, Chem Phys Chem. 8 (2007) 849–855, https://doi.org/10.1002/cphc.200600598.
[59] R. Momeni Feili, M. Dadsetani, R. Nejatipour, A. Ebrahimian, Electron Energy Loss Structures of Terminated Scandium and Hafnium MXene Monolayers from First-Principles Calculations, J. Electron. Mater. 49 (2020) 2502–2520, https://doi.org/10.1007/s11664-020-07946-w.
[60] S. Aydin, A. Tatar, Y.O. Ciftci, Some new members of MAX family including light-elements: Nanolayered Hf_2XY (X= Al, Si, P and Y Combining double low line B, C,

N), Solid State Sci. 53 (2016) 44–55, https://doi.org/10.1016/j.solidstatesciences.2015.10.010.
[61] B. Daoudi, A. Yakoubi, L. Beldi, B. Bouhafs, Full-potential electronic structure of Hf2AlC and Hf2AlN, Acta Mater. 55 (2007) 4161–4165, https://doi.org/10.1016/j.actamat.2007.03.011.
[62] M. Khazaei, A. Ranjbar, M. Arai, T. Sasaki, S. Yunoki, Electronic properties and applications of MXenes: a theoretical review, J. Mater. Chem. C. 5 (2017) 2488–2503, https://doi.org/10.1039/c7tc00140a.
[63] Z. Sheng, S. Wu, X. Dai, T. Zhao, Y. Hao, A first-principles study of hydrogen storage capacity based on Li-Na-decorated silicene, Phys. Chem. Chem. Phys. 20 (2018) 13903–13908, https://doi.org/10.1039/c8cp00722e.
[64] S. Haldar, S. Mukherjee, C.V. Singh, Hydrogen storage in Li Na and Ca decorated and defective borophene: A first principles study, RSC Adv. 8 (2018) 20748–20757, https://doi.org/10.1039/c7ra12512g.
[65] Y. Wen, F. Xie, X. Liu, X. Liu, R. Chen, K. Cho, B. Shan, Tunable H2 binding on alkaline and alkaline earth metals decorated graphene substrates from first-principles calculations, Int. J. Hydrogen Energy. 42 (2017) 10064–10071, https://doi.org/10.1016/j.ijhydene.2017.02.023.
[66] L.G. Arellano, F. de Santiago, Á. Miranda, F. Salazar, A. Trejo, L.A. Pérez, M. Cruz-Irisson, Hydrogen storage capacities of alkali and alkaline-earth metal atoms on SiC monolayer: A first-principles study, Int. J. Hydrogen Energy. (2020), https://doi.org/10.1016/j.ijhydene.2020.03.078.
[67] Y. Zhang, X. Cheng, Hydrogen storage property of alkali and alkaline-earth metal atoms decorated C24 fullerene: A DFT study, Chem. Phys. 505 (2018) 26–33, https://doi.org/10.1016/j.chemphys.2018.03.010.
[68] L. Si, C. Tang, The reversible hydrogen storage abilities of metal Na (Li, K, Ca, Mg, Sc, Ti, Y) decorated all-boron cage B28, Int. J. Hydrogen Energy. 42 (2017) 16611–16619, https://doi.org/10.1016/j.ijhydene.2017.05.181.
[69] A.M. Ali, N. Yahya, A. Mijinyawa, M.Y. Kwaya, S. Sikiru, Molecular simulation and microtextural characterization of quartz dissolution in sodium hydroxide, J. Pet. Explor. Prod. Technol. 10 (2020) 2669–2684, https://doi.org/10.1007/s13202-020-00940-2.
[70] C.N.M. Ouma, P.M. Modisha, D. Bessarabov, Catalytic dehydrogenation of the liquid organic hydrogen carrier octahydroindole on Pt (1 1 1) surface: Ab initio insights from density functional theory calculations, Appl. Surf. Sci. 471 (2019) 1034–1040, https://doi.org/10.1016/j.apsusc.2018.12.110.
[71] R.L.C. Akkermans, N.A. Spenley, S.H. Robertson, Monte carlo methods in materials studio, Mol. Simul. 39 (2013) 1153–1164, https://doi.org/10.1080/08927022.2013.843775.
[72] H.U. Nwankwo, L.O. Olasunkanmi, E.E. Ebenso, Experimental, quantum chemical and molecular dynamic simulations studies on the corrosion inhibition of mild steel by some carbazole derivatives, Sci. Rep. 7 (2017) 2436, https://doi.org/10.1038/s41598-017-02446-0.
[73] C.N. Moro Ouma, P. Modisha, D. Bessarabov, Insight into the adsorption of a liquid organic hydrogen carrier, perhydro-: I-dibenzyltoluene (i = m, o, p), on Pt, Pd and PtPd planar surfaces, RSC Adv. 8 (2018) 31895–31904, https://doi.org/10.1039/c8ra05800h.
[74] C. Baykasoglu, Z. Ozturk, M. Kirca, A.T. Celebi, A. Mugan, A.C. To, Effects of lithium doping on hydrogen storage properties of heat welded random CNT network structures, in: Int. J. Hydrogen Energy, Elsevier Ltd, 2016: pp. 8246–8255. https://doi.org/10.1016/j.ijhydene.2015.11.182 .
[75] S.R. Naqvi, T. Hussain, W. Luo, R. Ahuja, Metallized siligraphene nanosheets (SiC7) as high capacity hydrogen storage materials, Nano Res. 11 (2018) 3802–3813, https://doi.org/10.1007/s12274-017-1954-z.
[76] X. Jin, P. Qi, H. Yang, Y. Zhang, J. Li, H. Chen, Enhanced hydrogen adsorption on Li-coated B12C6N6, J. Chem. Phys. 145 (2016), 164301, https://doi.org/10.1063/1.4964394.
[77] K.M. Fair, X.Y. Cui, L. Li, C.C. Shieh, R.K. Zheng, Z.W. Liu, B. Delley, M.J. Ford, S. P. Ringer, C. Stampfl, Hydrogen adsorption capacity of adatoms on double carbon vacancies of graphene: A trend study from first principles, Phys. Rev. B - Condens. Matter Mater. Phys. 87 (2013), 014102, https://doi.org/10.1103/PhysRevB.87.014102.
[78] Y. Zhou, W. Chu, F. Jing, J. Zheng, W. Sun, Y. Xue, Enhanced hydrogen storage on Li-doped defective graphene with B substitution: A DFT study, Appl. Surf. Sci. 410 (2017) 166–176, https://doi.org/10.1016/j.apsusc.2017.03.057.
[79] Y. Liu, S. Gao, F. Lu, A. Yu, S. Song, H. Shi, Y. Mai, B. Liao, Hydrogen adsorption on Li decorated graphyne-like carbon nanosheet: A density functional theory study, Int. J. Hydrogen Energy 45 (2020) 24938–24946, https://doi.org/10.1016/j.ijhydene.2020.06.072.
[80] E. Beheshti, A. Nojeh, P. Servati, A first-principles study of calcium-decorated, boron-doped graphene for high capacity hydrogen storage, Carbon N. Y. 49 (2011) 1561–1567, https://doi.org/10.1016/j.carbon.2010.12.023.
[81] N. Song, Y. Wang, S. Ding, Y. Yang, J. Zhang, B. Xu, L. Yi, Y. Jia, The hydrogen storage behavior of Li-decorated monolayer WS2: A first-principles study, Vacuum 117 (2015) 63–67, https://doi.org/10.1016/j.vacuum.2015.03.034.
[82] N. Song, Y. Wang, Y. Zheng, J. Zhang, B. Xu, Q. Sun, Y. Jia, New template for Li and Ca decoration and hydrogen adsorption on graphene-like SiC: A first-principles study, Comput. Mater. Sci. 99 (2015) 150–155, https://doi.org/10.1016/j.commatsci.2014.12.016.
[83] R. Akilan, D. Ravichandran, S. Vinnarasi, R. Shankar, Adsorption of H2 and CO2 gas molecules on Li/Na decorated Si2BN nano-sheet for energy harvesting applications – A density functional study, Mater. Lett. 279 (2020) 128487, https://doi.org/10.1016/j.matlet.2020.128487.
[84] K. Alhameedi, A. Karton, D. Jayatilaka, T. Hussain, Metal functionalized inorganic nano-sheets as promising materials for clean energy storage, Appl. Surf. Sci. 471 (2019) 887–892, https://doi.org/10.1016/j.apsusc.2018.12.036.